3072 *Macromolecules* **2010**, *43*, 3072–3080
DOI: 10.1021/ma9026417

Macromolecules
ARTICLE

Simulation of Mechanically-Assembled Monolayers In Poor Solvent Using Discontinuous Molecular Dynamics

L. Anderson Strickland,* Carol K. Hall, and Jan Genzer

Received November 30, 2009; Revised Manuscript Received January 22, 2010

ABSTRACT: We present and discuss the results of discontinuous molecular dynamics simulations of mechanically assembled polymer layers chemically attached to flexible substrates under poor solvent conditions. Square-well chains of lengths comprising 20 to 100 units end-grafted to a hard surface at low density are compressed laterally at varying rates. Brush thickness depends on the interplay between solvent quality and the substrate compression rate. Brushes formed in poor solvents at fast compression rates are thinner and exhibit more heterogeneity in coverage than brushes formed in good solvents at slow compression rates. End-monomer trapping increases with increasing compression rate and/or decreasing solvent quality. By varying relaxation/compression rate, we can modify the effects of brush thickness hysteresis. Finally, we suggest a general blueprint for efficient formation of defect-free monolayers that might be followed by experimenters.

I. Introduction

Mechanically assembled monolayers (MAMs) represent substrate-anchored oligomer or polymer brushes fabricated by chemically attaching the polymers to a prestretched flexible substrate and then releasing the stretch. This process results in increasing the surface density of the grafted modifiers beyond values typically found when the molecules adsorb and assemble on rigid, nonstretchable supports. This method was originally proposed by Genzer et al. as an alternative to preparing dense polymer brushes by conventional "grafting-from" methods, i.e. atom transfer radical polymerization (ATRP).[1,2] In the original MAMs process,[3] semiflourinated organosilane polymers were allowed to self-assemble on tethering sites activated by ultraviolet/ozone (UV/O) treatment; the substrate was subsequently released, resulting in a dense thick brush of semiflourinated groups, whose surface density can be controlled by adjusting the amount of prestretching. Surfaces formed using this method exhibit no deterioration after 6 months exposure to deionized water — a quality highly desirable in coating of surfaces that would otherwise degrade under exposure to water.[3,4] Later efforts extended the MAMs technology from densifying small organic modifiers to long macromolecules chemically grafted to flexible substrates.[5] While the latter method was originally coined as MAPA (or mechanically assisted polymer assembly), for simplicity in this work, we combine both techniques under the same name, MAM.

In a previous paper we described results of a molecular simulation of the formation of long chain MAMs under good solvent conditions. The surface density of a model system of homopolymers attached to an impenetrable surface was systematically increased at a variety of surface release rates until a highly dense brush was achieved. Good solvent conditions were modeled by treating the monomer−monomer interactions as athermal.[6] The effect of varying chain length, reduced temperature and surface release rate on the structure of the monolayer was examined; no consideration was given to solvent quality. The thickness of MAMs brushes formed at slow release rates was consistent with the theory proposed by Alexander and de Gennes;[7−9] minor deviations from Murat and Grest simulations were observed at high formation rates due to polymer entanglement and at low chain length due to insufficient relaxation time.[10]

While in our previous work we neglected the effect of solvent quality, this parameter is known to play an important role in polymer behavior. Recent simulations-based research has focused on the effect of solvent quality on the collapse and conformation of homopolymers[11−14] and the thickness of polymer brushes at equilibrium, meaning at fixed surface density.[15−17] One would also expect that solvent quality affects the formation of MAMs and polymer brushes during the approach to equilibrium upon varying surface density of the grafted modifiers. Experimenters note a difficulty with the MAMs process in that quick compression of the monolayer leads often to buckling, which requires a relaxation period postrelease for equilibration. It is surmised that the competition between polymer−substrate bonding forces and polymer−polymer interaction forces can either cause polymers to detach or resist compression to high density. Clearly, for brushes in poor quality solvents, quick compression would affect the extension of the polymers away from the substrate, thereby indirectly affecting the monolayer's ability to achieve a denser, impenetrable brush via the densification process.

In this paper, we present the results of discontinuous molecular dynamics simulations of the compression of systems of polymers modeled as chains of square-well monomers in an attempt to mimic the formation of MAMs in lower quality solvent. Polymers of chain lengths 20, 50, and 100 are initially grafted to a hard surface at low density and allowed to equilibrate. These chains are then compressed laterally at varying rates to high surface density (to 1 monomer/area) in order to study the effects of chain length and compression rate on brush properties, i.e., density and polymer extension. By compressing at frequencies larger than the brush's equilibrium time-scale, we can assess how brush thickness and structure are affected during the MAMs formation process. By varying the system temperature (which controls solvent quality), we can assess the effect of solvent quality on brush thickness and structure. Finally, selected brushes are expanded back to low surface density, which enables us to study hysteresis effects on brush thickness and structure.

Highlights of this work are as follows. We present results for the monolayer thickness versus surface density as a function of

*Corresponding author.

 Published on Web 02/17/2010

compression rate and reduced temperature. We find that brush thickness can be directly controlled by adjusting the system reduced temperature and the surface compression rate. Brushes formed at temperatures below the theta temperature (T_Θ) and/or at low surface density exhibit significant brush degradation (gaps in polymer layer coverage and low brush thickness). Brushes formed at temperatures above T_Θ show increased thickness and enhanced orientation order. Specifically, the macromolecules are able to reach surface densities higher than brushes formed at low temperatures. The effectiveness of the MAMs formation process depends on whether or not the surface density is above the critical coverage density, ρ_c, which is defined to be the minimum surface density at which the surface is entirely covered by monomers. Longer chain systems suffer a slight deterioration in brush height as the surface density approaches the critical coverage density from below, even when formed by slow compression. Fast compression leads to end-monomer and chain trapping. Increasing the relaxation rate and/or reducing the temperature (thereby reducing solvent quality) leads to an increase in hysteresis effects in brush thickness. Finally, we show that for each compression rate, there exists a certain surface density value beyond which further compression attempts are likely to fail due to chain overlap or volume exclusion; from this behavior, we can infer that the optimal design for MAM fabrication is to intermittently decrease the compression rate as the surface density of the grafted macromolecules increases.

The remainder of the paper is organized as follows. In section II, we describe the discontinuous molecular dynamics method and outline the process for increasing surface density, ρ_a. Section III presents the simulation results at various chain lengths, compression rates and reduced temperature; the latter acts as a surrogate for solvent quality. We also analyze our results and suggest a generic set of guidelines for experimental fabrication of MAMs. Section IV provides a short summary of the results and a discussion.

II. Model and Methods

Discontinuous molecular dynamics (DMD) is a fast alternative to traditional molecular dynamics.[18] Unlike traditional molecular dynamics which employs a monomer−monomer interaction potential that is a continuous function of their separation (i.e., the Lennard-Jones potential), discontinuous molecular dynamics replaces monomer−monomer interactions with a square-well potential which incorporates short-range repulsions as well as long-range attractions.[19] The potential energy between nonbonded monomers is taken to be the square-well potential,

$$\begin{aligned} U(r) &= \infty, \quad r < \sigma \\ &= -\varepsilon, \quad \sigma \le r \le \lambda\sigma \\ &= 0, \quad r > \lambda\sigma \end{aligned} \tag{1}$$

where σ denotes the monomer diameter and λ is the width of the square-well interaction. To stay consistent with previous simulation work, σ and λ are set to 1.0 and 1.5, respectively. The advantage of DMD over traditional molecular dynamics is that monomers need not be moved incrementally at short regularly spaced time steps. Instead, one only need calculate the collision time, t_{ij}, at which a monomer reaches a discontinuity in its potential energy, $U(r)$, where it undergoes either repulsion with another monomer or enters/leaves the square-well interaction of another monomer. Collision times for all monomer−monomer pairs in the system are calculated, the minimum collision time for the system, t_c, is chosen, and all monomers are advanced forward according to

$$r_i(t + t_c) = r_i(t) + v_i(t_c) \tag{2}$$

where r_i and v_i represent the ith monomer's position and velocity, respectively. At this point, two monomers collide, their new postcollision velocities are calculated, and the steps described above are repeated.

Polymer systems are modeled in DMD as freely jointed chains comprising monomers bonded at a distance σ from one another. We use the Bellemans approximation which allows the bond length to fluctuate freely over the range $\sigma(1 \pm \delta)$, where δ is very small, for example 1/10th of σ.[20−22] The average bond length for neighboring monomers in a chain is approximately σ, which is close in architecture to tangentially connected monomers. Nonbonded monomers along a chain interact with the same energy, ε, as monomers on differing chains. The well-depth ε is set to $\varepsilon = 1$ in all simulations. We define the reduced temperature of the system, T^*, as $T^* \equiv k_B T/\varepsilon$. At high values of T^* the monomers acquire enough kinetic energy to escape the square-well interaction with their neighbor(s); this leads to chain stretching, mimicking good solubility conditions. At low values of T^*, the monomers are under the influence of their square-well interactions; as a result, the polymers collapse, just like under poor solubility conditions. Thus, the solubility of the polymers is measured by the reduced temperature, T^*. This implicit solvent model saves extra computational expense associated with introducing solvent molecules explicitly into the simulation.

Since the system's reduced temperature plays an important role, T^* must be carefully controlled throughout the simulation. This is accomplished through the use of an Andersen thermostat, which allows the system reduced temperature to fluctuate about the average value, T^*.[23] A ghost particle is created to collide with a randomly chosen monomer at a random collision time, t_g. The monomer's velocity is recalculated after the collision, ensuring that the velocities for all particles in the system are distributed according to a Gaussian distribution on T^*.

The model system comprises M polymer chains, each containing N square-well monomers, placed into a box having dimensions L_x and L_y (length and width, respectively). Periodic boundary conditions (PBC) are employed in the x- and y-directions; a monomer (or tethering point) which leaves the box on one side re-enters on the opposite size. PBC are not used in the z-direction. Backbone angles along the chain are free to fluctuate as long as there is no monomer−monomer overlap. Each chain is grafted at one end to a surface of area S (measured in units of σ^2), where the surface is designated $z = 0$. We define the surface density of the polymer chains as $\rho_a = M/S$. Tethering points for each chain are allowed to move along the surface but are not allowed to overlap. Because of the impenetrable surface, collision times between each monomer and the surface must also be calculated.

The formation of the dense mechanically assembled monolayer is modeled as a series of uniformly spaced compressions of the tethering surface. At prescribed collision numbers (for example, every 2000th monomer−monomer collision), we attempt to compress the box such that:

$$L_x(\text{new}) = L_x(\text{old})(1 - \delta_{L_x}) \tag{3}$$

$$L_y(\text{new}) = L_y(\text{old})(1 - \delta_{L_y}) \tag{4}$$

where δ_{L_x} and δ_{L_y} are very small (on the order of 1×10^{-5}). New monomer positions are calculated:

$$r_{ix}(\text{new}) = r_{ix}(\text{old})(1 - \delta_{L_x}) \tag{5}$$

$$r_{iy}(\text{new}) = r_{iy}(\text{old})(1 - \delta_{L_y}) \tag{6}$$

where r_i is the position of monomer i. If there are no monomer overlaps, the new positions are retained and the new surface density is calculated: $\rho_a = M/(L_{x,\text{new}} \times L_{y,\text{new}})$.

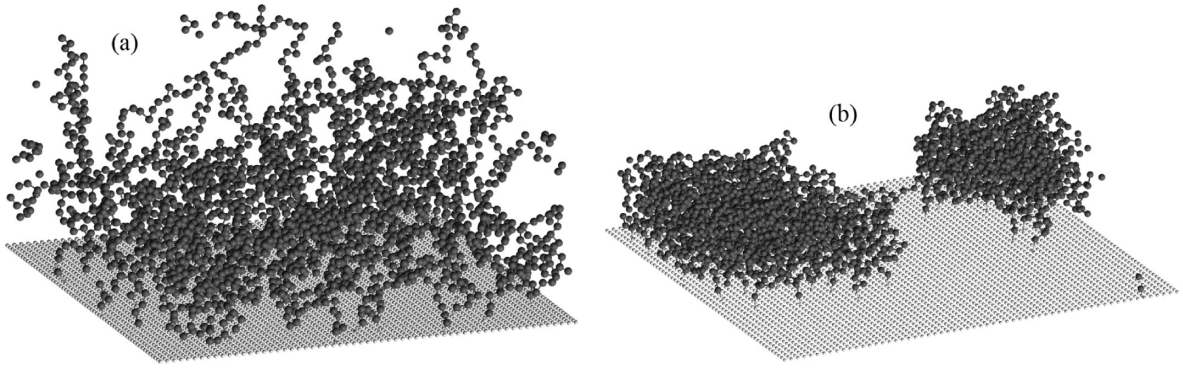

Figure 1. Comparison of monolayer snapshots for systems containing: (a) hard chain 50mers and (b) square-well chain 50mers at $T^* = 1.2$, which corresponds to poor-solvent conditions.

In this work, we present results from the compression and relaxation of the following systems: 20 20mers grafted at initial $\rho_a = 0.01, 0.03, 0.10$, and 0.20 monomers/area; 50 50mers grafted at initial $\rho_a = 0.01, 0.03$, and 0.10; and 25 100mers grafted at $\rho_a = 0.03$. The system temperature was varied over the range $T^* = 0.5$ to 8.0. After the systems were equilibrated at their initial surface density and temperature, compression moves (typically, every 500th, 2000th, or 10 000th collision) were attempted until the final surface density had been reached, $\rho_a = 1.000$, or until compression was no longer possible (discussed later). In between compression attempts, standard DMD moves were applied. At the end of selected compression runs, we expanded the surface back to its initial surface density, at a rate corresponding to the preceding compression rate, to investigate hysteresis effects and chain entanglement. Data were collected periodically on the polymer layer's mean-square radius of gyration, $\langle R_g^2 \rangle$, and the mean-square radius of gyration in the z-direction, $\langle R_{g,z}^2 \rangle$, defined respectively as

$$\langle R_g^2 \rangle = \langle \Sigma (r_i - r_{CM})^2 \rangle / N \tag{7}$$

$$\langle R_{g,z}^2 \rangle = \langle \Sigma (r_{zi} - r_{z,CM})^2 \rangle / N \tag{8}$$

where r_{zi} is the z-coordinate of the ith monomer position (r_i), $r_{z,CM}$ is the z-coordinate of the center of mass for i's corresponding chain (and its center of mass, r_{CM}) and the summation is averaged over all monomers N along each chain. Over the course of the monolayer compression, we also collected density profiles for all of the monomers in the systems, $\rho(z)$, and density profiles for the free ends, $\rho_E(z)$. This data was normalized according to $\int \rho(z)\, dz = 1$ for all systems. Even though most of the simulations were run several times, all but two of the figures in this paper show data for only one run since the point is to watch how the system evolves during the inherently nonequilibrium compression process. This also allows us to observe the effect of chain trapping. For some of the data presented here (Figures 9 and 10), three runs with randomly chosen initial configurations were conducted and the average values and error bars (calculated from the standard deviation) are shown. Results are given in detail in the next section.

III. Results

Decreasing solvent quality negatively affects monolayer properties and hence the fabrication of MAMs in two ways: (1) by reducing the coverage of the polymers on the surface and (2) by reducing the thickness of the monolayer. These two defects arise from the preferential monomer−monomer attraction relative to monomer−solvent contacts. This monomer−monomer attraction dominates at $T^* < T_\Theta$, where T_Θ, the theta temperature, is defined as the temperature at which the polymers act like ideal chains. On the basis of previous work by Grest and Murat[24] and Szleifer et al.,[25] $T_\Theta \sim 3.0$ for $\varepsilon = 1$.

To illustrate the effect of poor solvent quality (or $T^* < T_\Theta$), we present in Figure 1 snapshots of two systems, both composed of 50 50mers grafted to the same surface area. The left picture depicts the system in a good solvent (only core repulsion),[6] while the right picture shows the same system in a poor solvent, corresponding to reduced temperature $T^* = 1.2$. The effects of poor solubility lead to reduced thickness nearly 1/4 of that in a good solvent and a significant percentage of the tethering surface being uncovered by the polymer. The loss of surface coverage can be countered only by reaching densities above the critical density, ρ_c, as will be discussed later.

We begin by presenting results on the effect of solvent quality on the thickness of our monolayer systems. As has been previously reported by de Gennes[26] and others, the brush thickness, h, scales as $h \sim N\rho_a^{\alpha}$, where $\alpha = {}^2/_3$ and $\alpha = 2$ for good and poor solvent conditions, respectively. Thus, Figure 2 shows the logarithm of the mean-squared radius of gyration in the z-direction, $\langle R_{g,z}^2 \rangle$, a measure of monolayer thickness, normalized by chain length, N, as a function of the logarithm of surface density for systems of varying chain lengths; for comparison, we have also included the slopes of ${}^2/_3$ and 2 (good and poor solvent conditions). In Figure 2a, we present the results for 20mers compressed at reduced temperatures ranging from 1.0 to 4.0. (Because polymers shorter than 20mers show no significant change in monolayer thickness as a result of varying compression, they are not considered in this work.) For high T^*, an increase in surface density corresponds directly to an increase in $\langle R_{g,z}^2 \rangle$. At $T^* > T_\Theta$, polymers are somewhat extended; volume exclusion effects from increasing surface density extend them even further. Upon reducing T^* the film thickness decreases due to poor solvent conditions: monomers prefer one another over the implied solvent and thus do not extend as far as they do in good solvents. Transitioning from $T^* = 3.0$ (T_Θ) to $T^* = 2.0$ creates local inflections in the $\langle R_{g,z}^2 \rangle$ curve at low surface densities. In this region the substrate is not completely covered by the polymer layer. As will be shown later, despite the slow compression rate employed here, monolayer thickness can only increase *after* the collapsed chains first fill the space near the surface.

Variations in reduced temperature have a more pronounced effect on brush properties when longer chains are considered. Accordingly, in Figure 2b, we plot our results for 50mers at reduced temperatures from $T^* = 0.5$ to 8.0. For comparison, data for good solvent (a system of hard chains[6]) is included. As with the 20mers, the brush thickness increases with increasing surface density. However, when the temperature is lowered below $T_\Theta \approx 3.0$, the layer thickness decreases significantly. For example, at surface density $\rho_a \approx 0.3$ monomers/area, the poor solvent conditions at $T^* = 0.5$ and 2.0 lead to $\langle R_{g,z}^2 \rangle$-values

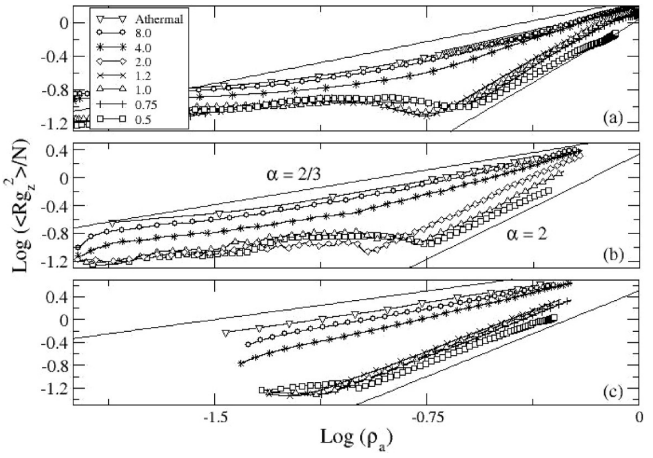

Figure 2. Mean-squared radius of gyration in the z-direction, $\langle R_{g,z}^2 \rangle$, as a function of surface density, ρ_a, for (a) 20 20mers, (b) 50 50mers and (c) 25 100mers at various reduced temperatures, T^*. Compressions were attempted once per 2000 monomer collisions.

approximately 15% and 33%, respectively, of the value observed under good solvent.

Also of interest in Figure 2b is the effect of reduced temperature on brush thickness, specifically at low surface densities. While in general increasing the surface density leads to an increase in monolayer thickness (especially at $T^* > T_\Theta$), compressing the monolayer when $T^* < T_\Theta$ has no effect on brush thickness over the surface density range 0.01 to approximately 0.2 monomers/area. This is due to the paucity of chain−chain contacts at low surface density which results in chains which act as independent globules; while monomers on the same chain interact, there is little interaction between monomers on differing chains. The minimum surface density at which a compression of the monolayer leads directly to an increase in monolayer thickness is defined as the impingement density, ρ_c, which is a function of the chain length and temperature. This density is the minimum density at which the neighboring chains, which adopt mushroom conformations characterized by radius of gyration R_g^2, just touch. It may be calculated by realizing that the area projected by a chain of radius of gyration R_g^2, onto a surface is πR_g^2. If these circles just touch, the fraction of area covered is the ratio of the area of a circle to that of a square, which is equal to $\pi R_g^2/4R_g^2 = \pi/4$. Likewise, it is equal to $\pi M R_g^2/S = \pi R_g^2 \rho_c$, where M is the number of chains and S is the surface area. Thus, $\rho_c = {}^1/_4 R_g^{-2}$. Realizing that the radius of gyration (R_g) for an isolated chain of length N in poor solvent scales as $N^{1/3}|\tau|^{-1/3}$, where $\tau \equiv (T^* - T_\Theta)/T_\Theta$,[27] upon substitution; this produces an equation for the impingement density:

$$\rho_c = (1/4)N^{-2/3}|\tau|^{2/3} \quad (9)$$

where N is the chain length. Given $T_\Theta \approx 3.0$, we estimate the impingement density for 50mers to be 0.008 monomers/area at $T^* = 2.0$, 0.014 monomers/area at $T^* = 1.0$ and 0.016 monomers/area at $T^* = 0.5$. In general, as reduced temperature decreases, impingement density increases. On the basis of the data in Figure 2b, we can calculate the actual impingement density (density at which the brush height increases with increasing density to the power $\alpha = 2$). The actual impingement densities are approximately 0.11 at $T^* = 2.0$, 0.16 at $T^* = 1.0$ and 0.17 at $T^* = 0.5$. Although the observed trend, ρ_c increases (or shifts further to the right) as T^* decreases, is the same as that predicted theoretically (eq 9), the observed values of impingement density during compression differ by 1 order of magnitude from the values predicted theoretically. As pointed out by Lai and Binder, at such a low reduced temperature (or poor solvent), the chains are not acting independently.[27] Evidence for this is shown in Figure 1b where the chains, allowed to move freely across the tethering surface, are clumped together rather than acting as individual, evenly spaced mushrooms. This clumping increases the open space on the surface and makes the impingement density higher than the value predicted by eq 9. To correct this effect, one would need to turn off the attraction between monomers on different chains. Thus, the reduction in solvent quality not only causes a significant loss in monolayer thickness, it also requires that a higher surface density be attained to reach full surface coverage.

The effects of solvent quality become even more pronounced for longer chains. In Figure 2c, we plot brush thickness results for 100mers at reduced temperatures from $T^* = 0.5$ to 8.0. For comparison, we include data on hard chains from Reference.[6] In general, there is loss of layer thickness for all T^* compared to the ideal solvent (hard chain) system. For 100mers at $T^* > T_\Theta$, we note an interesting trend: the rate of change in $\langle R_{g,z}^2 \rangle$ with increasing ρ_a *is the same* over the entire range of densities implying that MAMs formed at $T^* > T_\Theta$ compress as readily as brushes formed in ideal solvent. All losses in layer thickness for $T^* > T_\Theta$ systems result only from the loss in thickness during self-assembly at low surface density. We do not detect this trend for $T^* < T_\Theta$. Increasing ρ_a at $T^* < T_\Theta$ does not result in a linear increase in $\langle R_{g,z}^2 \rangle$ across all ρ_a. Thus, poor solvent affects the 100mer system in two ways: (1) causing extremely low brush thicknesses at the initial low ρ_a and (2) increased difficulty in compressing the brush to higher ρ_a.

Monolayer thickness can also be affected by the frequency of compression attempts. In Figure 3 we show the logarithm of $\langle R_{g,z}^2 \rangle$ normalized by chain length as a function of the logarithm of surface density. Since MAM formation is more interesting at poor solvent conditions, all of this data was collected at $T^* = 1.2$ (below T_Θ) where the effect of brush compression is most pronounced. In Figure 3a, we show our results for a system of 20mers at compression rates occurring with a frequency of 1 compression per 10 000th, 2000th, or 500th monomer collision. While there is some loss of monolayer thickness at faster compression rates (cf. 1/500) compared to slower compression rates, this degradation is no more than 5% and not significant.

Next, we examine the effect of surface release rate on the thickness of the monolayer at longer chain lengths. Figure 3b shows brush thickness data for 50mers for compression rates of 1 compression attempt every 500th, 2000th, and 10 000th monomer collision; for comparison, athermal or hard-chain data is included. The following trends are seen. First, at low densities, layer thickness is constant and independent of compression rate. The thickness increases only after the surface density has exceeded $\rho_a = \rho_c \approx 0.16$. Second, there is significant loss of thickness for all three rates compared to the hard-sphere (or good solvent) data, especially at low surface density. When surface density is low ($\rho_a \approx 0.01$) and $T^* < T_\Theta$, the monolayer contains large gaps in surface coverage (cf. Figure 1b). As the monolayer is compressed, the system must first fill these gaps before it can thicken into a brush. Thus, at low density, chains are less likely to interact, reducing chain extension. Still, even at high surface density, if $T^* < T_\Theta$, the chains will prefer one another relative to the solvent, thereby reducing layer thickness. Finally, compression rate has a direct effect on the thickness of a fully formed layer ($\rho_a \approx 1.000$). At $\rho_a \approx 1.000$, systems which are compressed more slowly (i.e., compression attempts every 2000th and 10 000th collision) experience losses in the value of $\langle R_{g,z}^2 \rangle$ of 8% and 4%, respectively, compared to the hardsphere system. Systems compressed more quickly (an attempt every 500th collision) experience an even greater reduction compared to the hard-chain case. Recall that for a system of 20mers there was a less than 5% loss of

thickness for all compression rates. Thus, as we increase the polymer length from 20 to 50, the degenerative effect of fast compression on monolayer thickness also increases.

In Figure 3c, we present brush thickness data for 25 100mers in poor solvent for compression rates of 1 compression attempt every 500th, 2000th, and 10 000th monomer collision as well as brush thickness for 50 100mers at a compression rate of 1 attempt every 10 000th monomer collision. We note first that the fastest compression rate (1 every 500th collision) coupled with the increase in chain length to 100 creates a system where compression cannot proceed beyond $\rho_a \approx 0.850$. This is most likely due to chain−chain entanglement or to chains being trapped underneath neighboring chains during compression. The 100mer system in poor solvent quickly finds itself "tied up" at high density with little chance to equilibrate. We should make it clear at this point that we use the term "entanglement" loosely here. We are purposefully compressing faster than the time it would take for the monolayer to equilibrate. Given sufficient time, the chains could have worked themselves free of one another, allowing compression to possibly continue. We have not allowed this time because the emphasis of this work is to determine the effect of poor solubility and quick compression rate on dense monolayer formation; that effect has been "entanglement" of the chains.

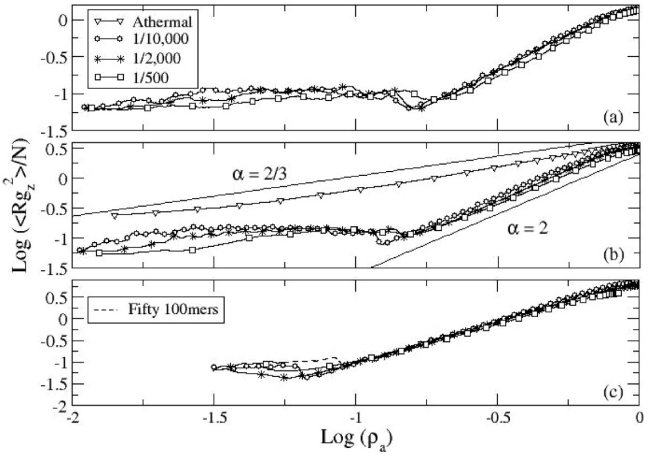

Figure 3. Mean-squared radius of gyration in the z-direction, $\langle R_{g,z}{}^2 \rangle$, as a function of surface density, ρ_a, for (a) 20 20mers, (b) 50 50mers and (c) 25 100mers at various compression rates and $T^* = 1.2$. By comparison, results for 50 100mers (---) at 1 compression attempt per 10,000 collisions are included in (c).

Next, we focus on the very low density region: $\rho_a \sim 0.06$ or log $(\rho_a) \sim -1.2$. Here, layer thickness for the system compressed every 10000th collision *decreases* as density increases from $\rho_a = 0.06$ to 0.065 [or, alternatively, as log (ρ_a) increases from -1.22 to -1.18]. We also show brushes at these two surfaces in Figure 4. Initially at $\rho_a = 0.06$ (left picture), there is not enough material to completely cover the surface due to poor solvent conditions (low T^*). Upon compressing the system to $\rho_a = 0.065$ (right picture), the empty space is filled up by the polymers. We hypothesize that at this point, the reduction in layer thickness is a result of individual chains sliding underneath neighboring chains; only as the surface density is further increased can volume exclusion effects force the majority of these chains to push away from the surface. If the compression rate is too high, some chains will become trapped, creating internal layer defects.

One last feature of interest in Figure 3c is the effect of increasing system size. The bulk of the data included in Figure 3c was collected on a system of 25 100mers. While periodic boundary conditions theoretically create an infinite system, it is of interest to ask if and how the relatively small system size considered here (25 100mers) affects the results obtained. Toward this end we performed compression simulations on a larger system: in this case, 50 100mers. (Attempts were made to simulate even larger systems but the time required to complete these compressions was prohibitive.) The system of 50 100mers (shown as a dashed line in Figure 3c) was initialized at a low grafting density. Compression moves were attempted every 10 000th monomer collision until $\rho_a \sim 1.00$. We found that brush thickness for the larger system is equivalent to the brush thickness in our slowest compression for most of the range of explored ρ_a except that the critical coverage density shifted to the right. In other words a higher density was required to cover the surface. We believe that, once again, this shift is because the chains do not act independently.

To this point we have focused only on the effect of increasing surface density on brush thickness; however, as the surface density increases and the chains extend outward, they also begin to align. Figure 5 shows the orientational order parameter of systems of various chain lengths as a function of surface density for three compression rates at $T^* = 1.2$. Here we define the orientational order parameter as $\langle \cos \theta_n \rangle = (z_n - z_{n-1})/|r_n - r_{n-1}|$, where $n = 0$ at the surface and θ_n is the angle between the bond formed by successive monomers in the chain and the z-axis;[6] we have averaged this parameter across all chains and bonds in the system. In Figure 5a, we present results for 50mers; for comparison, data for good solvent (hard-chain case) is also shown. As was the case for $\langle R_{g,z}{}^2 \rangle$, increasing surface density does

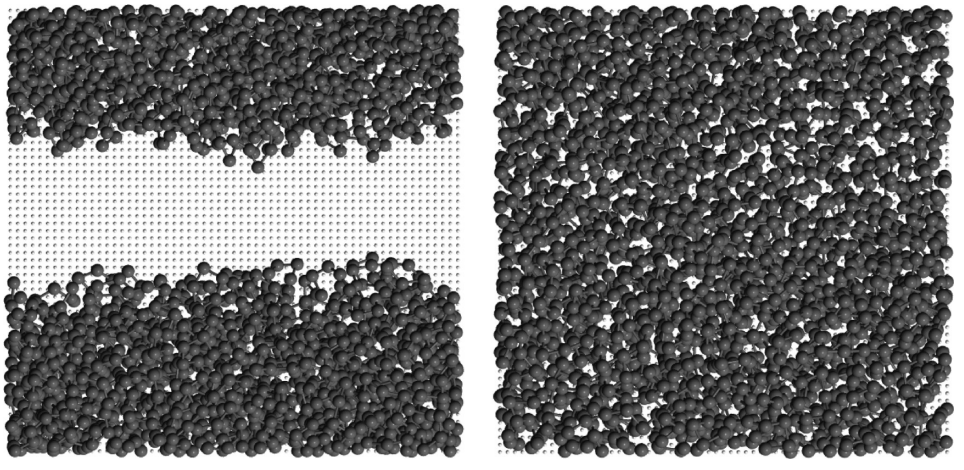

Figure 4. Top-down view of 25 100mers at $T^* = 1.2$ at a surface density less than the critical surface density (left, $\rho_a = 0.06$) and greater than critical surface density (right, $\rho_a = 0.065$). Compressions were attempted once per 10,000 monomer collisions.

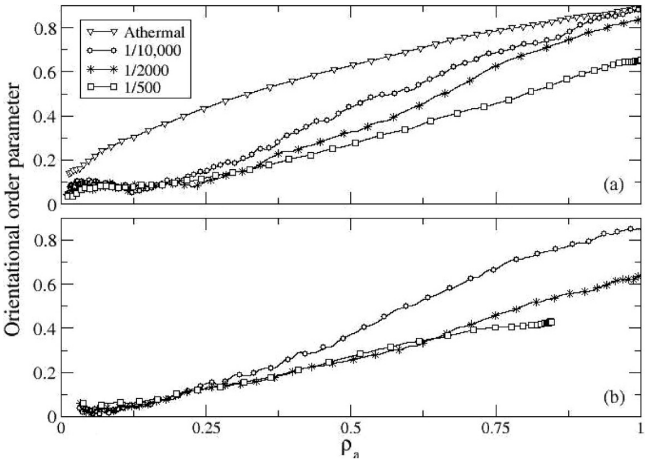

Figure 5. Orientation order parameter as a function of surface density for (a) 50 50mers and (b) 25 100mers at various compression rates and $T^* = 1.2$.

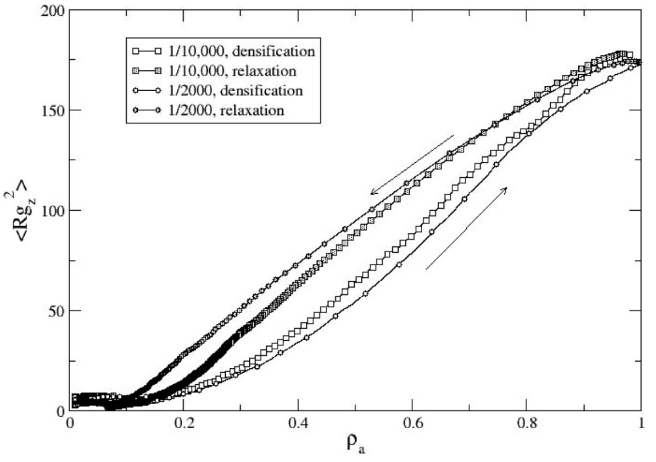

Figure 6. Mean-squared radius of gyration hysteresis data for 50 50mers at $T^* = 1.2$ compressed/decompressed at two different rates.

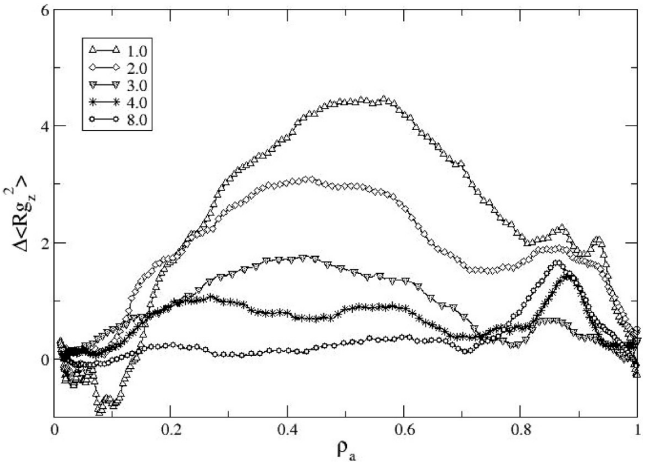

Figure 7. Mean-squared radius of gyration hysteresis data for 20 20mers compressed/decompressed at various reduced temperatures, T^*. Compressions were attempted once per 2000 monomer collisions.

not affect polymer ordering until $\rho_a \approx 0.3$. Beyond this point, further compression increases ordering. Increasing the compression rate results in a loss of order. Only the slowest compression (1 compression attempt every 10,000th monomer collision) allows the system to align itself structurally as well as the hard-sphere system does at the highest surface densities. Similar to 50mers, 100mer data presented in Figure 5b show that increasing the compression rate reduces the system ordering significantly. By comparison at $\rho_a \approx 1.000$, $\langle \cos \theta_i \rangle = 0.82$ and 0.62 for the systems compressed 1 every 10000th and 2000th monomer collision, respectively. One can back-calculate that the bonded monomer angles in the system which was compressed every 2000th collision are, on average, about 17° more parallel to the surface than the bonded monomer angles for the good solvent; this is patently undesirable in designing a well-ordered brush.

Up to this point, we have examined only the effects of variations in solvent quality and compression rate on the order and thickness of monolayers as surface density is increased. However, it has been suggested by experimenters that one advantage of MAMs over systems where self-assembly occurs naturally is that the surface density is not permanently set. To this end, one could easily restretch the surface to lower the surface coverage. In Figure 6, we graph $\langle R_{g,z}^2 \rangle$ versus surface density for 50mers compressed every 10,000th (---) and every 2000th (-■-) collisions to $\rho_a \approx 1.000$ and *then relaxed back* at the same rate to $\rho_a \approx 0.01$. Two effects are of importance here. First, increasing the compression/relaxation rate increases the hysteresis in brush thickness: at $\rho_a \approx 0.5$, $\langle R_{g,z}^2 \rangle$ during relaxation phase for the faster-formed brush is about 67% higher than $\langle R_{g,z}^2 \rangle$ seen during compression phase. In comparison, the $\langle R_{g,z}^2 \rangle$-value during relaxation phase for the slower-formed brush is only 30% higher than that seen during the compression phase. Second, increasing the compression/relaxation rate increases the range in ρ_a over which hysteresis occurs. For example, when a compression was attempted every 10 000th collision, the surface density had to be relaxed to $\rho_a \approx 0.12$ to remove hysteresis effects (monolayer thickness equivalent for compressed and relaxed systems). By comparison, to remove hysteresis effects from the system with compressions/relaxations every 2000th collision, surface density had to be reduced to $\rho_a \approx 0.06$, i.e., nearly the initial surface density $\rho_a \approx 0.01$. Fast compression/relaxation leads to losses in layer thickness *that are harder to remove*. Thus, there exist trade-offs: Quick MAM compression reduces time to form a dense layer but only at the expense of reduced layer ordering and thickness. Should the monolayer need to be "reset", quick MAM formation requires that the monolayer be relaxed to a surface density that is lower than would have been the case with slow compression. Results for 20mers and 100mers follow this same trend as that discussed for 50mers and are thus not presented here.

Alternately we present hysteresis effects at various values of the reduced temperature instead of the compression rate. Figures 7 and 8 show the $\Delta\langle R_{g,z}^2 \rangle = \langle R_{g,z}^2 \rangle_{\text{relaxation}} - \langle R_{g,z}^2 \rangle_{\text{compression}}$ versus surface density for 20mers and 100mers, respectively, at various T^*. Both figures follow the same general trend. Lowering T^*, especially to values below T_Θ, results in large $\Delta\langle R_{g,z}^2 \rangle$-values, primarily centered on $\rho_a \approx 0.50$. In contrast, one notices at $T^* \approx 8.0$, $\Delta\langle R_{g,z}^2 \rangle$ for 20mers (cf. Figure 7) is essentially zero and for 100mers is much smaller than for the other temperatures. It should be noted that for 20mers (cf. Figure 7), there are two inflections in the hysteresis loop that need to be explained: A positive deviation at high ρ_a /low T^* and a negative deviation at low ρ_a/low T^*. At high ρ_a /low T^*, relaxation from high surface density initially creates gaps near the tail-end of the monomers. Chains that had been trapped by the compression can momentarily extend, causing a small fluctuation in the hysteresis loop. Further relaxation eliminates this effect, as chain segments are pulled down to the surface. At low ρ_a/low T^*, we detect the opposite effect. When the surface is initially compressed, chains are isolated and adopt a relaxed conformation independent of surface density until further compression introduces neighboring polymers. When the system returns to low surface density

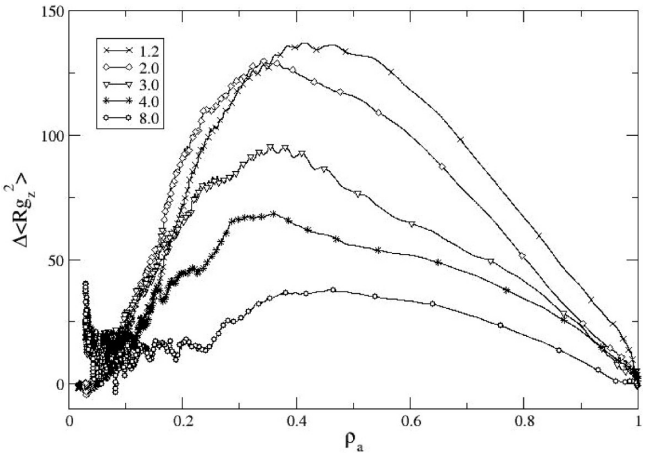

Figure 8. Mean-squared radius of gyration hysteresis data for 25 100mers compressed/decompressed at various reduced temperatures, T^*. Compressions were attempted once per 2000 monomer collisions.

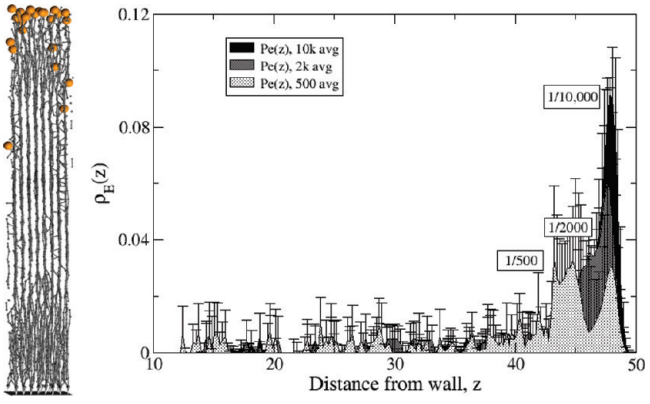

Figure 9. End-monomer density profile for 50 50mers compressed to surface density $\rho_a = 1.0$ at $T^* = 1.2$ and various compression rates averaged over three runs. Picture on the left depicts a side view of monolayer formed during slow compression.

via relaxation, chains are no longer isolated — they typically bundle together in a mushroom conformation, adopting $\langle R_{g,z}^2 \rangle$ lower than the value seen when they were isolated during compression phase. This behavior results in a negative $\Delta\langle R_{g,z}^2 \rangle$-value.

Next, we focus on the location of the end-monomer unit. Experimenters want to tailor this monomer to allow fine-tuning of the barrier properties of the resulting high-density MAM. It is thus essential that end-monomers be at or near the exposed free surface. Figure 9 shows the end-monomer density profile for 50mers as a function of compression rate; this data has been averaged over three runs. Slow compression (1 every 10 000th monomer collision) tends to create layers with a large majority of the end monomers far from the tethering surface, a situation desirable in the MAM fabrication. This outcome can be seen in the inset to Figure 9 which shows a side-view of the brush with enlarged end-monomers; here, most chain ends are grouped near the outer edge. By comparison, fast compression (1 every 500th collision) leaves more chain ends trapped within the layer. Thus, not only does fast compression reduce the integrity of the layer and its ordering, it reduces the effectiveness of the barrier surface. The data in Figure 10 show the chain end density profile for 100mers. As was seen with 50mers, slow compression of 100mers creates layers whose end-monomers are located far from the tethering surface (which is highly desirable); fast compression of 100mers leads to even more end-monomer trapping compared to

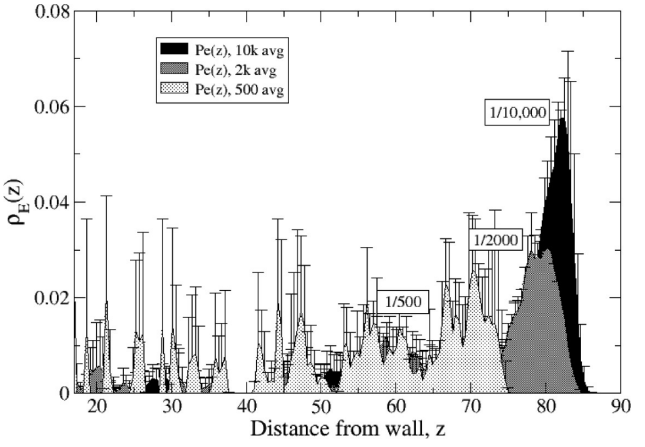

Figure 10. End-monomer density profile for 25 100mers compressed to surface density $\rho_a \approx 0.75$ at $T^* = 1.2$ and various compression rates averaged over three runs.

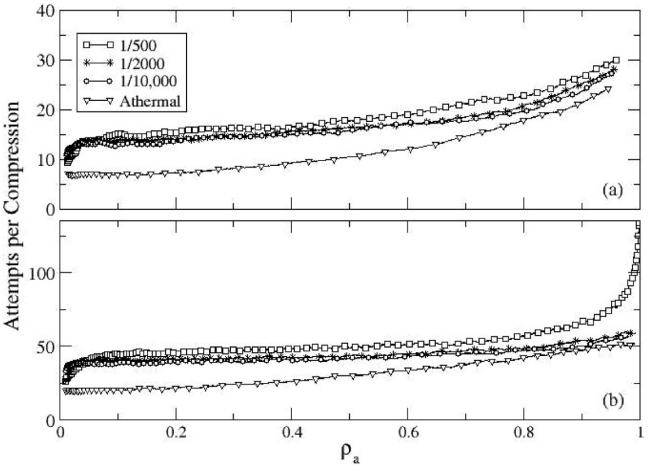

Figure 11. Number of attempts per successful compression at $T^* = 1.2$ for (a) 20 20mers and (b) 50 50mers as a function of surface density at various compression rates.

50mers. There exists a direct correlation: as we increase the compression rate, the probability of finding an end-monomer trapped in the monolayer increases.

Data to this point were given in terms of *attempted* compression rate. A significant percentage of compression attempts, especially at the higher surface densities and longer chain lengths, were unsuccessful due to monomer−monomer overlap. To gain a better understanding of the amount of time required for formation of MAMs in poor solvent, it is useful to determine the actual success rate of compression.

In Figure 11a, we present the number of attempts required for each successful compression of 20mers versus surface density at different compression rates. Starting with an initial surface density of 0.03 monomers/area, we attempt a compression once per 10 000th, 2000th, or 500th collision. For comparison, we include equivalent data for the compression of 20mers under good solvent conditions (hardsphere data).[6] Even at low surface density, poor solvent systems require nearly twice as many compression attempts relative to good solvent systems. In general, compression becomes more difficult with increasing surface density of the grafts. In addition, faster compressions are harder to carry out than slower compressions over the entire range of ρ_a. It should be noted, though, that the disparity between the success of compression attempts in poor and good solvent reduces as surface density increases; high surface coverage slows compression regardless of solvent quality.

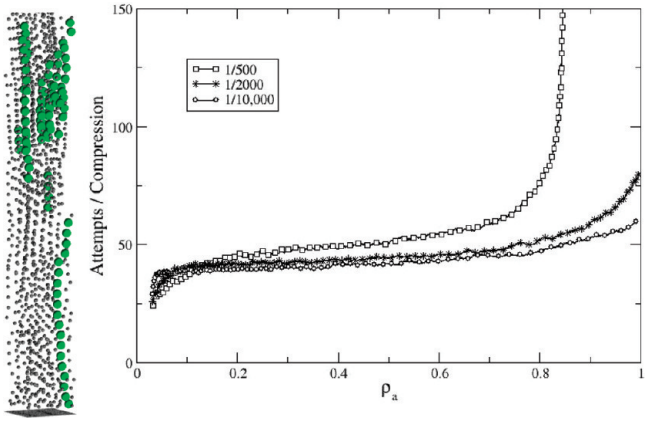

Figure 12. Number of attempts per successful compression at $T^* = 1.2$ for 25 100mers as a function of surface density at various compression rates. Picture on the left depicts trapped chains near the tethering surface for fastest compression case.

In Figure 11b, we plot the number of attempts per successful compression as a function of surface density for 50mers. Although the trends are similar to those observed for 20mers, it should be noted that the number of attempts per compression for 50mers is much higher than that for 20mers. At low surface density, compression attempts in systems under poor solvent conditions are about half as successful relative to those performed in good solvent systems; compression becomes harder as surface density increases; and the disparity between poor and good solvent conditions diminishes at high surface density. One new feature shows up in the 50mer compression data. Specifically, we see that the increase in chain length has caused the number of attempts per compression for the fastest compressed system to spike past surface densities $\rho_a \approx 0.90$. The compression has reached a "speed limit": Trying to compress faster than 1 attempt every 500th collision would become extremely difficult, while compressing at a rate slower than once every 500th collision (for example, every 2000th) is relatively easy. This behavior is reflected also in Figure 12, which shows the number of attempts per compression for 100mer systems. As stated previously, the combination of long chain length and high compression rate leads to considerable underpinning of grafted chains. The system reaches a state where chains are so entangled in the layer that further compression is either impossible or would require an unrealistic amount of time. For example, one chain from the configuration of the fastest compressed system at $\rho_a \approx 0.85$ has been isolated in the Figure 12 inset. The chain, shown as larger spheres, bends back on itself at least five times indicating that further compression would clearly be impossible for this one chain.

One focus of this work has been on how simulation can guide experimenters in the fabrication of MAMs. Clearly, a major consideration in MAMs production is the time it takes for MAMs to form. To date, MAMs formation on the small scale has consisted of steady-state surface compression. After deposition and self-assembly of the polymers, the surface is either allowed to snap back quickly, resulting in surface ripples which are then equilibrated over time (say, a week) or allowed to slowly relax, avoiding the surface ripples but requiring a significant amount of time for formation.[28] Obviously, a middle ground can be found, where the surface compression rate changes over time or, more importantly, as surface density changes. In Figure 13 we plot the rate of change of the surface density with time versus reduced time, t^*, at the three compression rates for 20mers where reduced time is defined to be $t^* = t/\sigma(k_BT/m)^{1/2}$. When we attempt a compression once every 10 000 or 2000 monomer collisions, the same trend occurs: relatively slow compression

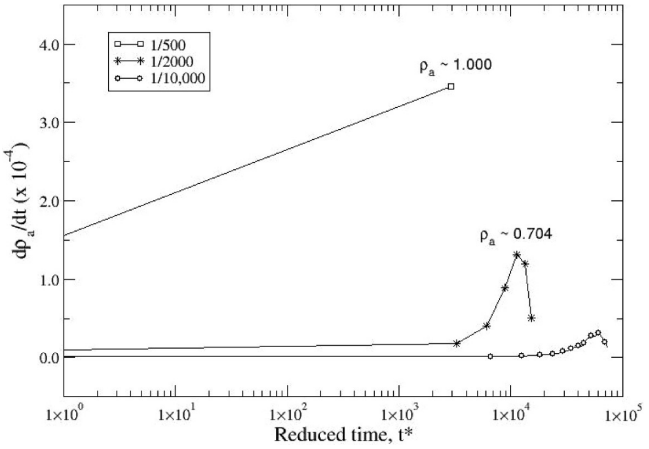

Figure 13. Change in surface density per change in reduced time ($d\rho_a/dt^*$) for 20 20mers as a function of reduced time at $T^* = 1.2$ and various compression rates.

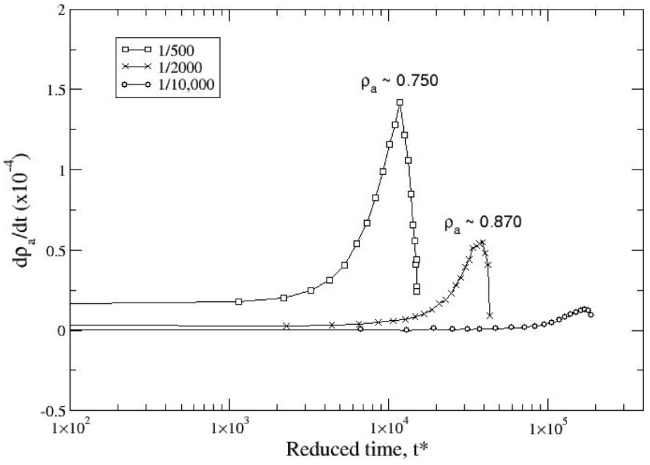

Figure 14. Change in surface density per change in reduced time ($d\rho_a/dt^*$) for 50 50mers as a function of reduced time at $T^* = 1.2$ and various compression rates.

initially, followed by increasing success, a peak around $\rho_a \approx 0.7$ to 0.8, followed by reduced success in compression until $\rho_a = 1.000$ is reached. The fastest compression rate (1 attempt every 500th collision) shows no such trend, rising steadily from $\rho_a = 0.030$ to $\rho_a = 1.000$. On the basis of the data presented in Figure 3a, which showed relatively little layer thickness loss due varying compression rate, faster compression rates should be carried out for all chain lengths less than 20 monomers.

The data in Figure 14 depict the rate of change of the surface density with time versus reduced time for 50mers at $T^* = 1.2$. There is a peak at around $\rho_a \approx 0.75$ for the fastest compression rate (every 500th collision). Slower compression rates of 1 attempt every 2000th and 10000th collision show success rates that peak at $\rho_a \approx 0.78$ and 0.87, respectively; all three systems reach completion at $\rho_a = 1.000$, regardless of compression rate. Because of the significant loss of $\langle R_{g,z}^2 \rangle$ for 50mers at fast compression rates (cf. Figure 3b), it might be advisible to vary the compression rate over time or over the course of compression. One could start with fast compression (for example, compressing every 500th monomer collision) reaching the maximum at $\rho_a \approx 0.75$, then reduce the compression rate to 1 attempt every 2000th collision, reaching another maximum rate around $\rho_a \approx 0.782$ and then further reduce the compression rate until $\rho_a = 1.000$. In this way, experimenters might enhance monolayer thickness and structure but at the expense of reducing the rate of formation. Moving to longer chain lengths shows the same trend. Figure 15

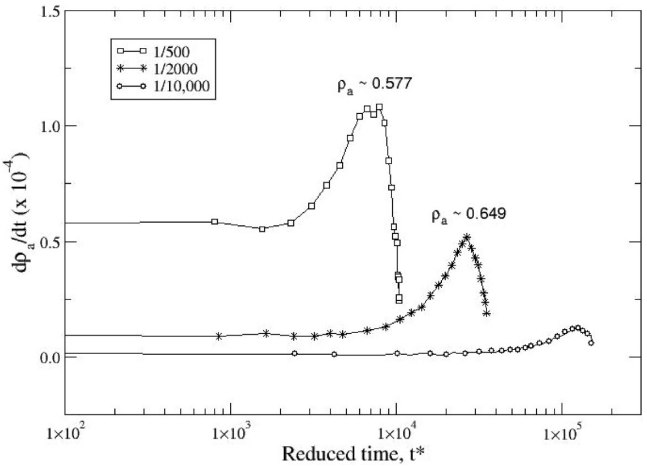

Figure 15. Change in surface density per change in reduced time ($d\rho_a/dt^*$) for 25 100mers as a function of reduced time at $T^* = 1.2$ and various compression rates.

shows $d\rho_a/dt$ for 100mers. The compression success rate for the fastest compressed system (1 attempt every 500th collision) peaks around $\rho_a \approx 0.58$ while compressing every 2000th collision leads to a success rate that peaks around $\rho_a \approx 0.65$. As described above for 50mers, in order to create dense and defect-free layers one would need to periodically reduce the compression rate at surface densities higher than the peak success rate (or specifically here, at surface densities beyond $\rho_a \approx 0.58$). On the basis of these observations, we conclude that experimenters must begin reducing the compression rate at a lower surface density as chain length increases.

IV. Conclusions

We have presented results for the compression and relaxation of surfaces containing tethered chains composed of square-well monomers, thereby mimicking the formation of mechanically assembled monolayers under poor solvent conditions. Compression/relaxation rates were varied, as was system temperature (or, equivalently, solvent quality). Poor solvent quality presents two major drawbacks for monolayers: (1) loss of surface coverage and (2) loss of monolayer order/thickness. Loss of surface coverage can be countered by starting the compressions at surface densities in excess of the critical coverage density or by compressing slowly, thereby allowing the chains sufficient time to avoid entangling. Along with an increase in chain entanglement, fast compression rates lead to a reduction of overall monolayer order and chain extension, thereby reducing monolayer thickness. Thus, there is a trade-off between having fast compressions and having ordered, thick and therefore impenetrable monolayers. We also noted that when highly compressed surfaces were relaxed, significant hysteresis effects were present for fast relaxation rates at low reduced temperatures, especially at $T^* < T_\Theta$. Our end-monomer density profiles indicate that the number of monolayer defects increased as the compression rate increased. It is surmised that higher compression rates would lead to a loss of barrier properties. Finally, we compared the actual compression rates in the poor solvent systems to the actual compression rates in the good solvent systems and suggested a course of action for experimenters to follow when fabricating MAMs on a large scale.

Acknowledgment. We thank Amit Goyal for thoughtful discussions. This work was supported by the Director, Office of Energy Research, Office of Basic Sciences, Chemical Science Division of the U.S. Department of Energy under Grant No. DE-FG05-91ER14181. J.G. thanks the Office of Naval Research for financial support through Grant No. N00014-07-0253.

References and Notes

(1) Jones, D. M.; Brown, A. A.; Huck, W. T. S. Surface-Initiated Polymerizations In Aqueous Media: Effect Of Initiator Density. *Langmuir*. **2002**, *18*, 1265–1269.
(2) Koh, K.; Sugiyama, S.; Morinaga, T.; Ohno, K.; et al. Precision Synthesis Of A Fluorinated Polyhedral Oligomeric Silsesquioxane-Terminated Polymer And Surface Characterization Of Its Blend Film With Poly(Methyl Methacrylate). *Macromolecules* **2005**, *38*, 1264–1270.
(3) Efimenko, K.; Genzer, J. Creating Long-Lived Superhydrophobic Polymer Surfaces Through Mechanically Assembled Monolayers. *Science* **2000**, *290* (5499), 2130–2133.
(4) Genzer, J.; Efimenko, K. Recent Developments In Superhydrophobic Surfaces And Their Relevance To Marine Fouling: A Review. *Biofouling* **2006**, *22* (5), 339–360.
(5) Wu, T.; Efimenko, K.; Genzer, J. Preparing High-Density Polymer Brushes By Mechanically Assisted Polymer Assembly. *Macromolecules* **2001**, *34*, 684–686.
(6) Strickland, L. A.; Hall, C. K.; Genzer, J. Simulation Of Mechanically Assembled Monolayers And Polymers In Good Solvent Using Discontinuous Molecular Dynamics. *Macromolecules* **2008**, *41*, 6573–6581.
(7) de Gennes, P.-G. Conformations Of Polymers Attached To An Interface. *Macromolecules* **1980**, *13*, 1069–1075.
(8) Alexander, S. Adsorption Of Chain Molecules With A Polar Head A-Scaling Description. *J. Phys.* **1977**, *38*, 983–987.
(9) de Gennes, P.-G. *Scaling Concepts in Polymer Physics*; Cornell University Press: Ithaca, NY, 1979.
(10) Murat, M.; Grest, G. S. Structure Of A Grafted Polymer Brush - A Molecular-Dynamics Simulation. *Macromolecules* **1989**, *22*, 4054–4059.
(11) Chang, R.; Yethiraj, A. Solvent Effects On The Collapse Dynamics Of Polymers. *J. Chem. Phys.* **2001**, *114*, 7688–7699.
(12) Taylor, M. P.; Ichida, S. Conformation Of A Polymer Chain In Explicit Solvent: A Solvation Potential Approach. *J. Polym. Sci. B.* **2007**, *45*, 3319–3326.
(13) Opps, S. B.; Polson, J. M.; Abou Risk, N. Discontinuous Molecular Dynamics Simulation Study Of Polymer Collapse. *J. Chem. Phys.* **2006**, *125*, 194904.
(14) Taylor, M. P. Conformation Of A Polymer Chain In Solution: An Exact Density Expansion Approach. *J. Chem. Phys.* **2004**, *121*, 10757–10765.
(15) Yakubov, G. E.; Loppinet, B.; Zhang, H.; et al. Collective Dynamics Of An End-Grafted Polymer Brush In Solvents Of Varying Quality. *Phys. Rev. Lett.* **2004**, *92*, 115501.
(16) Li, T. L.; Park, K. N. A. Monte Carlo Simulation Of Grafted Poly(ethylene oxide) Chains. *Comp. Theor. Polym. Sci.* **1999**, *11* (2), 133–142.
(17) Kent, M. S.; Majewski, J.; Smith, G. S.; et al. Tethered Chains In Poor Solvent Conditions: An Experimental Study Involving Langmuir Diblock Copolymer Monolayers. *J. Chem. Phys.* **1999**, *110*, 3553–3565.
(18) Alder, B. J.; Wainwright, T. E. In *International Symposium on Transport Processes In Statistical Mechanics*; Prigogine, I., Ed.; Interscience: New York, 1956.
(19) Allen, M. P.; Tildesley, D. J. *Computer Simulation of Liquids*. Clarendon Press: Oxford, U.K., 1987.
(20) Rapaport, D. C. Molecular-Dynamics Simulation Of Polymer-Chains With Excluded Volume. *J Phys A: Math Gen.* **1978**, *11*, L213–L217.
(21) Rapaport, D. C. Molecular-Dynamics Study Of A Polymer-Chain In Solution. *J. Chem. Phys.* **1979**, *71*, 3299–3303.
(22) Bellemans, A.; Orban, J.; van Belle, D. Molecular-Dynamics Of Rigid And Non-Rigid Necklaces Of Hard Disks. *Mol. Phys.* **1980**, *39*, 781.
(23) Andersen, H. C. Molecular-Dynamics Simulations At Constant Pressure And-Or Temperature. *J. Chem. Phys.* **1980**, *72*, 2384.
(24) Grest, G. S.; Murat, M. Structure Of Grafted Polymeric Brushes In Solvents Of Varying Quality - A Molecular-Dynamics Study. *Macromolecules* **1993**, *26*, 3108–3117.
(25) Szleifer, I.; O'Toole, E. M.; Panagiotopoulos, A. Z. Monte-Carlo Simulation Of The Collapse-Coil Transition In Homopolymers. *J. Chem. Phys.* **1992**, *97*, 6802–6808.
(26) deGennes, P.-G. Conformations of Polymers Attached To An Interface. *Macromolecules* **1980**, *13*, 1069–1075.
(27) Lai, P.-Y.; Binder, K. Structure And Dynamics Of Polymer Brushes Near The Theta Point - A Monte-Carlo Simulation. *J. Chem. Phys.* **1992**, *97*, 586–595.
(28) Genzer, J.; Efimenko, K. Unpublished data.